A minority of foci or pan-nuclear apoptotic staining of γH2AX in the S phase after UV damage contain DNA double-strand breaks

Sebastien de Feraudy[1], Ingrid Revet, Vladimir Bezrookove, Luzviminda Feeney, and James E. Cleaver[1]

Department of Dermatology, University of California, San Francisco, CA 94115

Contributed by James E. Cleaver, February 22, 2010 (sent for review January 5, 2010)

UV irradiation induces histone variant H2AX phosphorylated on serine 139 (γH2AX) foci and high levels of pan-nuclear γH2AX staining without foci, but the significance of this finding is still uncertain. We examined the formation of γH2AX and 53BP1 that coincide at sites of double-strand breaks (DSBs) after ionizing radiation. We compared UV irradiation and treatment with etoposide, an agent that causes DSBs during DNA replication. We found that during DNA replication, UV irradiation induced at least three classes of γH2AX response: a minority of γH2AX foci colocalizing with 53BP1 foci that represent DSBs at replication sites, a majority of γH2AX foci that did not colocalize with 53BP1 foci, and cells with high levels of pan-nuclear γH2AX without foci of either γH2AX or 53BP1. Ataxia-telangiectasia mutated kinase and JNK mediated the UV-induced pan-nuclear γH2Ax, which preceded and paralleled UV-induced S phase apoptosis. These high levels of pan-nuclear γH2AX were further increased by loss of the bypass polymerase Pol η and inhibition of ataxia-telangiectasia and Rad3-related, but the levels required the presence of the damage-binding proteins of excision repair xeroderma pigmentosum complementation group A and C proteins. DSBs, therefore, represent a small variable fraction of UV-induced γH2AX foci dependent on repair capacity, and they are not detected within high levels of pan-nuclear γH2AX, a preapoptotic signal associated with ATM- and JNK-dependent apoptosis during replication. The formation of γH2AX foci after treatment with DNA-damaging agents cannot, therefore, be used as a direct measure of DSBs without independent corroborating evidence.

DNA damage response | replication | UV irradiation | apoptosis | 53BP1

To maintain the integrity of genomic information under threat of DNA damage, cells employ a range of responses including DNA repair, replication bypass, recombination, cell-cycle checkpoints, and senescence or apoptosis (1, 2). These responses are described by the all-embracing concept of the DNA damage response (DDR) (1). DNA double-strand breaks (DSBs) are important but not the only starting lesion for the DDR.

In eukaryotic cells, the DDR is rapidly initiated by the PI3K kinases ataxia-telangiectasia and Rad3-related (ATR) and ataxia-telangiectasia mutated kinase (ATM) (3, 4). ATR is recruited to single-stranded DNA regions at stalled replication forks in response to replication stress (5–8); ATM is activated primarily in response to DSBs (3, 9–11). ATR and ATM phosphorylate serine threonine protein kinase and CHK2, respectively, which activate cell-cycle checkpoints and p53, leading to a p53-dependent apoptotic pathway (12). This kinase cascade phosphorylates serine 139 and tyrosine 142 of the histone variant H2AX. After ionizing radiation accumulates in foci, phosphorylated H2AX (γH2AX) serine threonine protein kinase colocalizes with other markers of DSBs (53BP1, pNBS1, MDC1, and Brca1) in immunofluorescent microscopy (IF) (13–16). γH2AX foci are frequently adopted as quantitative markers for DSBs in IF (17, 18). However, the exact correspondence between γH2AX and DSBs remains uncertain (19, 20), especially after UV irradiation. Whereas DSBs are made directly by ionizing radiation and some carcinogenic chemicals, they arise only indirectly as a result of the action of repair or degradation of arrested replication forks after UV irradiation (21, 22). Moreover, UV irradiation induces γH2AX distributions ranging from foci to high-level uniform pan-nuclear staining depending on stages of the cell cycle (20–22). The UV-induced γH2AX response is, therefore, complex, and the extent to which DSBs are involved is uncertain. Instead, γH2AX may represent different branches of the DDR, involving nucleotide excision repair (NER), the bypass polymerase Pol η, DNA replication arrest, recombination, or apoptosis (15, 19, 20, 22–25).

Therefore, we addressed the following questions. What fraction of UV-induced γH2AX foci represents DSBs? Which kinases mediate UV-induced high levels of pan-nuclear γH2AX? What does this signal represent? To answer these questions, we examined γH2AX and 53BP1, which coincide at sites of DSBs after ionizing radiation (13, 18, 26, 27), as a measure of DSBs after UV irradiation. Cells were also treated with etoposide, which is a topoisomerase II inhibitor that causes DSBs during S phase (28–30). Etoposide was used as an independent measure for the detection of S phase DSBs. We assessed the involvement of ATR, ATM, and JNK in both γH2AX formation and apoptosis during S phase after UV irradiation. DSBs were found in less than one-half of UV-induced γH2AX foci, and they were not detected within high levels of pan-nuclear γH2AX, which represents a pre-apoptotic signal associated with ATM- and JNK-dependent apoptosis during replication.

Results

UV Irradiation Induces γH2AX Foci During S Phase but Few Colocalize with 53BP1. The presence of UV-induced DSBs was determined by costaining for γH2AX (18) and 53BP1 (13, 16) after UV irradiation or etoposide (50 μM) using IF and flow cytometry. We used human fibroblasts immortalized with human telomerase reverse transcriptase or transformed with SV40 (Table S1). Cells were harvested from 0 min to 20 h after a dose of 20 J/m^2, two times the dose required to saturate the number of γH2AX foci (22) (Fig. 1).

After UV irradiation, we identified three main populations of cells with foci that persisted for at least 20 h after exposure (Fig. 1*A*): (*i*) cells displaying large γH2AX foci that colocalized with large 53BP1 foci (Fig. 1*A*, column D) similar to those observed after treatment with etoposide or ionizing radiation (Fig. S1), which indicates the site of DSBs, (*ii*) cells displaying small γH2AX foci in the absence of 53BP1 foci (Fig. 1*A*, column B), and (*iii*) rare cells displaying 53BP1 foci that did not colocalize with γH2AX foci (Fig. 1*A*, column C). The relative percentages of these cell populations (Fig. 1 *A* and *D* and Tables 1 and 2) and the mean numbers of foci per nucleus (Fig. 1 *B* and *C*) fluctuated over time.

Author contributions: S.d.F., I.R., and J.E.C. designed research; S.d.F., I.R., L.F., and J.E.C. performed research; S.d.F, I.R., V.B., and J.E.C. analyzed data; and S.d.F., I.R., V.B., and J.E.C. wrote the paper.

The authors declare no conflict of interest.

[1]To whom correspondence may be addressed. E-mail: sdeferaudy@partners.org or jcleaver@cc.ucsf.edu.

This article contains supporting information online at www.pnas.org/cgi/content/full/1002175107/DCSupplemental.

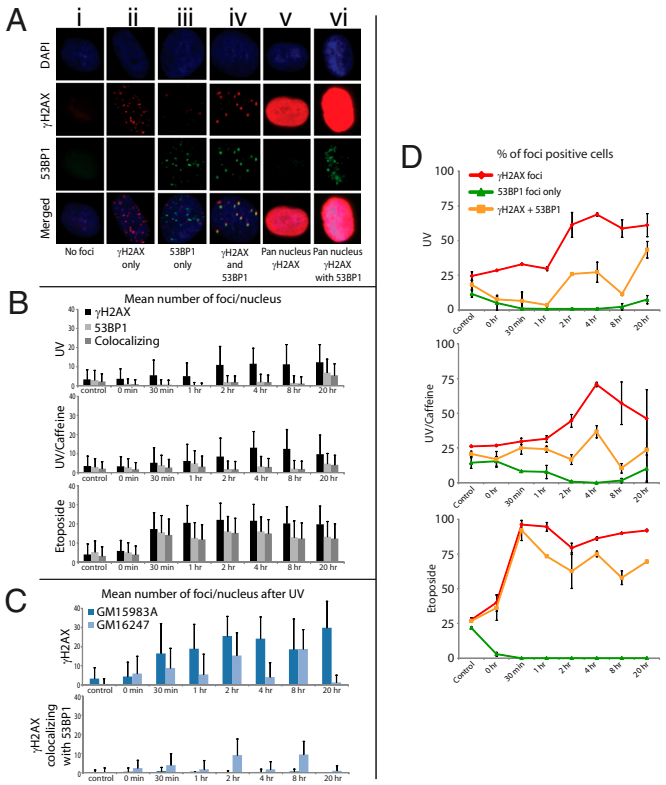

Fig. 1. Kinetics of γH2Ax and 53BP1 formation by IF after UV irradiation with or without caffeine and treatment with etoposide in normal fibroblasts GM5659T or SV40-transformed XPC cells. Cells were UV irradiated (20 J/m2) and incubated with or without caffeine (1 mM) or treated with etoposide (50 μM), and they were harvested between 0 and 20 h and stained for γH2Ax and 53BP1. (*A*) Images of the cell populations scored. Column A, no foci; column B, cell with multiple γH2Ax foci without 53BP1 foci; column C, very rare cell displaying 53BP1 foci without γH2Ax foci; column D, cell displaying both γH2Ax and 53BP1 foci; E, cell displaying high levels of pan-nucleus γH2Ax without 53BP1 foci; column F, cell displaying high levels of pan-nucleus γH2Ax with 53BP1 foci. (*B*) Mean and SEs ($n = 2$) of γH2Ax and 53BP1 foci per nucleus after UV irradiation with or without caffeine and treatment with etoposide in normal (GM2659T) cells. (*C*) Mean and SEs ($n = 2$) of γH2Ax and 53BP1 foci per nucleus after UV irradiation of XPC and XPC cells corrected by XPC cDNA. (*D*) Time course for percent of labeled cells stained for total γH2Ax, 53BP1, and coincident foci as a function of time after UV or etoposide exposure.

The percentage of cells displaying large γH2AX foci that colocalized with 53BP1 (Fig. 1*A*, column D, and Fig. 1*D Top*) was lower than the percentage of cells displaying small γH2AX foci in the absence of 53BP1 foci (Fig. 1*A*, column B, and Fig. 1*D*). Furthermore, analysis of the numbers of foci per nucleus after UV irradiation (Fig. 1 *B* and *C*) showed that the mean numbers of large γH2AX foci that colocalized with 53BP1 were lower than the numbers of small γH2AX foci that did not colocalize with 53BP1 (Fig. 1*B*). In fact, in each nucleus, only about 20% of γH2AX foci colocalized with 53BP1 foci between 2 and 8 h after UV irradiation (Table 1). Treatment with caffeine (31, 32) did not increase the percentage of UV-induced γH2AX foci colocalizing or not with 53BP1 foci (Fig. 1 *B* and *D Middle* and Table 2). Thus, after UV irradiation, γH2AX foci that colocalized with 53BP1 foci occurred at a lower number per nucleus and in fewer cells than γH2AX foci that did not colocalize with 53BP1 foci. In comparison, the majority (66%) of γH2AX foci colocalized with 53BP1 foci between 2 and 8 h after etoposide (Table 1).

We also observed very rare populations of cells displaying 53BP1 foci in the absence of γH2AX foci (Fig. 1 *A*, column C, and *D*). The percentage of this cell population remained constant over time and most likely corresponded to a background signal. In fact, the mean numbers of 53BP1 foci per nucleus matched the mean numbers of γH2AX foci that colocalized with 53BP1 foci (Fig. 1 *B* and *D* and Table 1), indicating that most 53BP1 foci occurred in the presence of γH2AX foci at DSBs (13, 18, 26). In summary, UV irradiation induced numerous γH2AX foci but less than one-half colocalized with 53BP1. Thus, DSBs represented only a small fraction of the total number of UV-induced γH2AX foci.

High Levels of Pan-Nuclear γH2AX Are Induced by UV Damage in the Absence of 53BP1 Foci. After UV irradiation (20 J/m^2), a subpopulation of cells displayed high levels of uniform pan-nuclear γH2AX staining without identifiable γH2AX foci (Fig. 1 *A*, column E, and *E* and Figs. S1 and S2). Nuclei with pan-nuclear γH2AX contained proliferating cell nuclear antigen (PCNA) (Fig. S2), indicating that the cells were in S phase but did not contain 53BP1 foci (Fig. 1*A*, column E and Figs. S1 and S2); 53BP1 foci colocalized only with the large γH2AX foci induced by UV irradiation, ionizing radiation, or etoposide (Fig. 1 *A*, column D, *B*, and *D* and Figs. S1 and S2). Therefore, high levels of pan-nuclear γH2AX were induced by UV damage during replication in the absence of detectable DSBs.

ATM and JNK Mediate UV-Induced High Levels of Pan-Nuclear γH2AX During S phase. Flow cytometry analysis of γH2AX expression during the cell cycle indicated increased levels of γH2AX in all phases of the cell cycle of human fibroblasts (GM637 and GM056 59hTERT) 4 h after exposure to UV (20 J/m^2) (Fig. 2 and Figs. S3). G1 cells had 2- to 3-fold more γH2AX than did nonirradiated cells. Cells in early and late S phase contained 5- to 6-fold more γH2AX than did nonirradiated cells. Cells spread throughout S phase contained at least 10-fold more γH2AX than nonirradiated cells, and they represented 18% of S phase cells (Fig. 2*A*). This signal persisted for up to 20 h after UV (Fig. 1). Based on the intensity of signal, the cells that displayed UV-induced high levels of γH2AX during S phase by flow cytometry corresponded to the population of cells that displayed UV-induced pan-nuclear γH2AX during S phase by IF (Fig. 1*A*, column E, and Figs. S1 and S2).

Table 1. Relative frequencies of γH2Ax and 53BP1 foci per cell after exposure to UV (20 J/m^2), UV plus caffeine (20 J/m^2 and 1 mM caffeine), or etoposide (50 μM) in normal GM5659T cells

	γH2Ax foci	53BP1 foci	γH2Ax and 53BP1 foci (coincident)	(γH2Ax + 53BP1)/γH2Ax
Control	3.6 ± 7.2	3.8 ± 5.0	2.6 ± 4.1	70.5%
UV	11.3 ± 9.5	1.9 ± 3.8	1.7 ± 3.5	15.2%
UV plus caffeine	11.4 ± 9.5	2.5 ± 4.6	2.3 ± 4.3	20.0%
Etoposide	21.3 ± 8.7	15.0 ± 8.1	14.2 ± 7.8	66.4%

Numbers were calculated from the mean numbers of foci per cell at 2, 4, and 8 h after exposure (Fig. 1*B*). The frequencies of total γH2Ax foci (first column) were subjected to paired comparisons and were significantly different ($P < 0.0001$) except for UV versus UV plus caffeine ($P = 0.5712$). The frequencies of coincident γH2Ax and 53BP1 foci (third column) were subjected to paired comparisons and were not significantly different ($P < 0.0001$) except for control versus UV plus caffeine, which had a marginal difference ($P = 0.0495$).

Table 2. Relative frequencies of γH2Ax and 53BP1 foci per cell after exposure to UV (20 J/m^2) in SV40-transformed XPC cells GM15983A and XPC cells corrected with *XPC* cDNA GM16247

	γH2Ax foci*	γH2Ax and 53BP1 foci (coincident)†	(γH2Ax + 53BP1)/γH2Ax
GM15983A	22.8 ± 12.6	0.3 ± 0.9	1.7%
GM16247	12.7 ± 9.9	9.4 ± 6.6	50.5%

Numbers were calculated from the mean numbers of foci per cell at 2, 4, and 8 h after exposure (Fig. 1*D*). All *P* values were calculated from mean of number of γH2AX, 53BP1, and colocalized foci from three time points (2, 4, and 8 h) using a Student *t* test with the assumption that there was unequal variance.
*$P < 0.0001$.
†$P < 0.0001$.

The high levels of pan-nuclear γH2AX did not represent the aggregate signal of nuclear foci. After ionizing radiation (2 Gy), γH2AX was uniformly increased by a factor of 2 in all phases of the cell cycle, representing the aggregate signal of nuclear foci (15, 33); however, no high levels of pan-nuclear γH2AX were detected by flow cytometry or IF (Fig. 2*E* and Fig. S1).

Inhibition of ATM by KU55933 (50 μM) reduced pan-nuclear γH2AX from 17.9% to 0.1% in GM637 cells (Fig. 2*A*). In GM0 5659hTERT cells, wortmannin, a less-specific inhibitor of ATM, and KU55933 reduced pan-nuclear levels of γH2AX from 12.3% to 5.1% and 1.7%, respectively (Fig. 2). The efficiency of KU55933 was confirmed in Western blots (Fig. 3). Consistent with these findings, UV irradiation of ataxia-telangectesia (A-T) cells, which are naturally deficient in ATM, did not induce high levels of γH2Ax during S phase (Fig. 2*D*). Similarly, inhibition of JNK by the chemical inhibitor SP600125 (Fig. 3 *A*–*C*) reduced UV-induced high levels of γH2AX during S phase from 17.9% to 5.3% (Fig. 2*A*). These results show that ATM and JNK mediate UV-induced high levels of γH2AX during S phase. In contrast, treatment with caffeine (1 mM) that inhibits the ATR–CHK1 pathway (31, 32) increased the levels

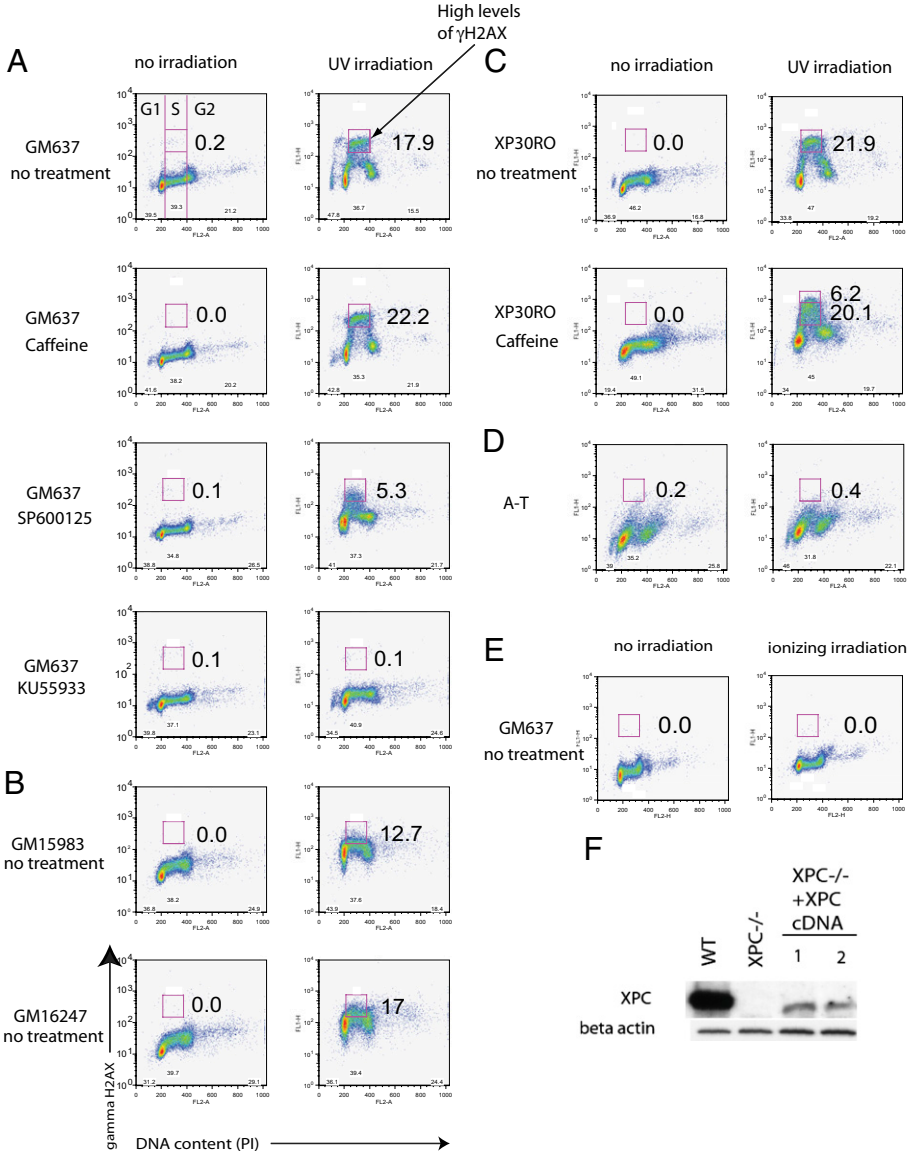

Fig. 2. Mediation of high levels of UV-induced γH2Ax during S phase by ATM and JNK. Flow cytometry profiles of hTERT- and SV40-transformed fibroblasts stained for nuclear expression of γH2Ax and propidium iodide (PI) to measure DNA content and identify the G1, S, and G2 phases of the cell cycle (separated by vertical lines). Cells were harvested 4 h after UV irradiation (20 J/m^2). The boldface box in S phase indicates the gate for high levels of γH2Ax. Numbers represent percentages of cells with high levels of γH2Ax in S phase. Data are representative of at least three independent experiments. (*A*) Levels of γH2Ax in wild-type (GM637) cells in the presence of caffeine, the JNK inhibitor SP600125, and the ATM inhibitor KU55933. (*B*) Levels of γH2Ax in XPC-deficient (GM15983) and corrected (GM16247) cells. (*C*) Levels of γH2Ax in xeroderma pigmentosum variant (XP-V) cells (XP30RO) grown with or without caffeine. (*D*) Levels of γH2Ax in hTERT-transformed ATM-deficient cells. (*E*) Levels of γH2Ax in normal cells after 2 Gy ionizing irradiation. (*F*) Western blot or normal (WT:GM637), XPC-deficient (GM15983), and two corrected cells (1, GM16247; 2, GM16248); the low level of XPC expression was sufficient to restore resistance to UV.

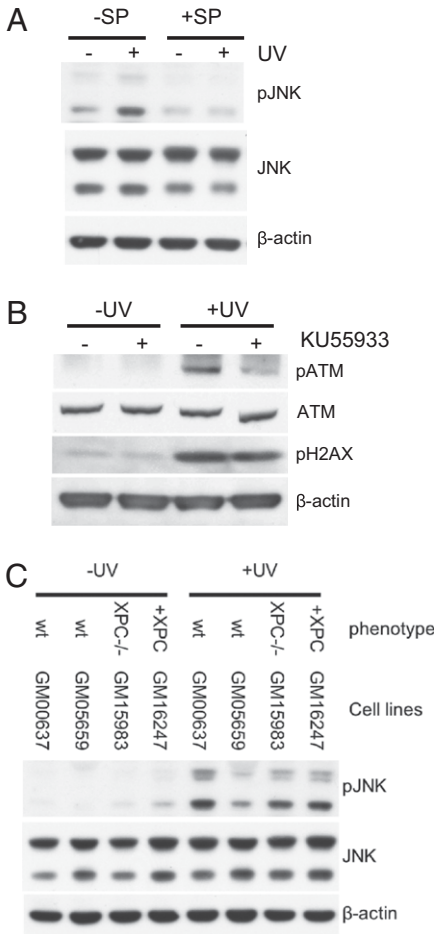

Fig. 3. Western blots showing specificity of pJNK and pATM inhibitors and loss of XPC in cells irradiated with UV (20 J/m^2) and harvested after 4 h. (*A*) Normal cells exposed to the JNK inhibitor SP600125 showing reduction in pJNK. (*B*) Normal cells exposed to the ATM inhibitor KU55933 showing inhibition of pATM and a small reduction in γH2Ax. (*C*) Normal (GM637 and GM5659), XPC (GM15983), and XPC-corrected (GM16247) cells showing lower levels of pJNK in hTERT-transfected (GM5659) than SV40-transformed (GM637) normal cells. XPC-deficient cells showed lower levels of pJNK with little increase after correction. This is consistent with the low levels of XPC expression (Fig. 2*F*), although the levels were sufficient to restore cell survival after UV.

of pan-nuclear γH2AX from 17.9% to 22.2% in GM637 cells (Fig. 2*A*) and from 12.3% to 14.3% in GM5659hTERT cells (Fig. S3).

Role of Xeroderma Pigmentosum Complementation Group C Protein in Generating UV-Induced High Levels of γH2Ax During S Phase. Xeroderma pigmentosum complementation group C protein (XPC), the main DNA damage-recognition protein for global NER, binds to undamaged single-stranded DNA opposite lesions (34). In XPC cells that lack this protein, the number of cells expressing UV-induced high levels of γH2AX during S phase was reduced from 17.9% to 12.7% in SV40 transformed cells (Fig. 2*A* and *B*) and from 12.3% to 1.1% in hTERT-transformed fibroblasts (Fig. S3). These results were confirmed by complementation of XPC-deficient cells with a cDNA coding for *XPC* (Fig. 2*F* and Fig. S3), which almost completely restored the number of cells expressing UV-induced high levels of γH2AX during S phase from 12.7% to 17% (Fig. 2*B*). Similarly, in the absence of xeroderma pigmentosum complementation group A (XPA), which binds to DNA photoproducts after XPC, the number of cells expressing pan-nuclear γH2AX was reduced from 12.3% to 0.0% (Fig. S3). Our results show that early steps in NER, involving XPC and XPA, are required for high levels of pan-nuclear γH2AX during S phase.

IF analysis showed that complementation of XPC-deficient cells (GM15983A) with *XPC* cDNA (GM16247) increased the number of γH2AX foci that colocalized with 53BP1 foci (Figs. 1*C* and 2*F* and Table 2). The fraction of γH2AX that costained with 53BP1 was higher in complemented (SV40) cells than in normal (hTERT) cells (Tables 1 and 2), which is an indication of the variability of the fraction of DSBs according to cell type; this remains no more than one-half of all γH2AX foci. These results suggest that reexpression of XPC increases the number of DSBs at replication forks (Table 2).

Pol η Deficiency Increases both the Fraction of Cells Displaying UV-Induced High Levels of γH2AX and the Intensity of γH2AX During S Phase. Pol η is the main polymerase for bypassing DNA photoproducts in the S phase (24, 25). In Pol η-deficient cells (XP-V), the fraction of cells displaying pan-nuclear γH2AX during S phase was higher than in GM637 cells (Fig. 2 *A* and *C*) (21.9% versus 17.9%). Treatment of XP-V cells with caffeine increased the fraction of cells with pan-nuclear γH2AX even more (from 21.9% to 26.3%) (Fig. 2*C*). Treatment of XP-V cells with caffeine also increased the intensity of γH2AX during S phase; 6.2% of XP-V cells treated with caffeine had greater intensity of UV-induced high levels of γH2AX than did XP-V cells or GM637 cells without caffeine (Fig. 2*C*). Therefore, Pol η deficiency, combined with caffeine during S phase, increases both the fraction of cells displaying UV-induced high levels of γH2AX and the intensity of γH2AX.

UV-Induced Apoptosis During S Phase Is Mediated by ATM and JNK. UV damage causes apoptosis in SV40-transformed cells (35). Because the stimulation of pan-nuclear γH2AX by caffeine is reminiscent of the S phase toxicity of caffeine (32, 36), we hypothesized that pan-nuclear γH2AX is an early signal of UV-induced S phase apoptosis. Consequently, inhibition of ATM and JNK should reduce UV-induced S phase apoptosis, whereas caffeine should increase it, especially in XP-V cells. To test this hypothesis, we measured UV-induced S phase apoptosis in SV40 transformed cells by quantifying the fraction of cells detached from the growth surface after UV irradiation (35). We proved that, in response to UV irradiation, SV40-transformed cells detached from their growth surface in S phase (judged by their BrdU content) and subsequently, showed DNA degradation and protein poly(ADP ribose) polymerase (PARP-1) cleavage (Fig. S4) (35), whereas detachment was prevented by the apoptosis inhibitor carbobenzoxy-valyl-alanyl-aspartyl-[O-methyl]-fluoromethylketone (ZVAD) (Fig. 4*A*) (35). We found that about 25% of S phase GM637 underwent apoptosis 20 h after UV. Inhibition of ATM with KU55933 and inhibition of JNK with SP600125 (Fig. 3) reduced this percentage to 7% and 13%, respectively ($P < 0.001$) (Fig. 4*B*). The fraction of UV-induced apoptotic S phase cells was higher in XP-V cells than in normal cells (Fig. 4*C*), and it was further increased in the presence of caffeine (Fig. 4*C*), as previously reported (35). Therefore, both UV-induced S phase apoptosis and high levels of pan-nuclear γH2AX were mediated by ATM and JNK and increased by caffeine or Pol η deficiency.

Discussion

Three salient features issue from these experiments regarding the role of γH2AX during the UV DDR: (*i*) less than one-half of the total number of γH2AX foci that are detected after UV irradiation were associated with DSBs, (*ii*) UV-induced high levels of pan-nuclear γH2AX represented preapoptotic signals that were also not associated with DSBs, and (*iii*) most γH2AX is produced during DNA replication by ATM- and JNK-dependent phosphorylation and not by ATR. Each of these topics will be

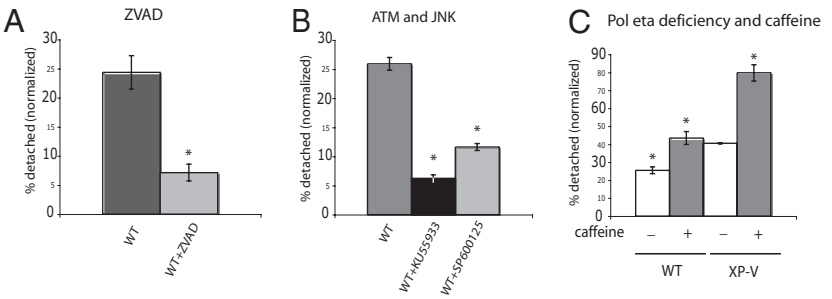

Fig. 4. Inhibition of UV-induced apoptosis by inhibitors of caspase 3, pATM, and pJNK, and the effect of caffeine and loss of Pol η. Normal (GM637) and XP-V (XP30RO) cells were irradiated with UV (20 J/m^2) and supplemented with ZVAD (25 μM), KU55933 (50 μM), SP600125 (100 μM), or caffeine (1 mM) for 20 h. The percentage of apoptotic cells released from the substrate was calculated as the number of detached cells divided by the total number of attached plus detached cells. (*A*) Reduction of apoptotic cells in the presence of ZVAD. (*B*) Reduction of apoptotic cells in the presence of KU55933 or SP600125. (*C*) Increase in apoptotic cells because of caffeine or loss of Pol η in normal (WT: GM637) or XP-V (XP30RO) cells. Significant differences are indicated by asterisks. $P < 0.005$ with Student *t* test assuming unequal variances or ANOVA. Error bars denote SEM ($n \geq 3$).

discussed in turn. For this study, we have depended on inhibition of phosphorylation by chemical inhibitors of ATR, ATM, and JNK and cell lines deficient in ATM (A-T), NER (XPA, XPC), or bypass replication (XP-V, Pol η). Caffeine has been identified as an inhibitor of the ATR–CHK1 pathway in vivo (32), although its K_1 for ATM is lower than for ATR in vitro (31).

Evidence that UV-induced DSBs represented less than one-half of UV-induced γH2AX foci was based on the fraction of γH2AX foci per cell that colocalized with 53BP1 foci (Tables 1 and 2). In each nucleus, between 2 and 8 h after UV irradiation, only about 20% of γH2AX foci colocalized with 53BP1 foci in wild-type cells and 50% in XP-C cells corrected with *XPC* cDNA (Tables 1 and 2). The percentage increased 20 h after UV irradiation, indicating that UV-induced DSBs were late events. Caffeine did not change the numbers of foci or their coincidence, indicating that γH2AX foci were not produced by ATR. In contrast, we found that after etoposide, 66% of γH2AX foci coincided with 53BP1, indicating a higher fraction of DSBs (28–30). After X-rays, all DSBs were reported to coincide with γH2AX foci (37). Fork breakage was reduced in the absence of the NER protein XPC (Fig. 1*C*), suggesting a role for excision repair at the replication forks.

The significance of UV-induced γH2AX foci in the absence of 53BP1 foci is not clear. During replication, they may represent unbroken stalled forks subject to further processing or more complex structures. Low doses of etoposide induced γH2AX foci associated with covalent DNA-Topo II complexes without DSBs, but the fraction associated with DSBs increased at higher doses (30). The number of γH2AX foci per nucleus after UV damage, 20–30 at most, was much less than the number of replication forks per cell estimated at 10^3 to 10^4 (38). Either replication forks clustered in groups of up to 100 forks per cluster or many arrested forks did not register as γH2AX foci.

UV irradiation also generated high levels of pan-nuclear γH2AX without foci during the S phase that did not contain 53BP1 foci. These results were not artifacts, because colocalized γH2AX and 53BP1 foci at the sites of DSBs were detected simultaneously in the neighboring cells after UV irradiation (Fig. S1) and in the majority of cells treated with etoposide (29, 30) or ionizing radiation (13–16). Our findings indicated that these cells represented a preapoptotic signal; they preceded and paralleled the percentage of UV-induced apoptotic cells, which was shown by cell detachment, PARP1 cleavage, and DNA degradation (Figs. 2–4 and Fig. S4). In addition, inhibition of ATM or JNK reduced levels of pan-nuclear γH2AX and reduced UV-induced S phase apoptosis in parallel. In contrast, inhibition of ATR by caffeine in XP-V cells dramatically increased the intensity of both UV-induced pan-nuclear γH2AX (Fig. 2*C*) and UV-induced S phase apoptosis (Fig. 4*C*).

Similar high levels of pan-nuclear γH2AX have been observed as a result of activation of the tumor necrosis factor-related apoptosis-inducing ligand (TRAIL) pathway (39). TRAIL-induced pan-nuclear γH2AX was suppressed by the apoptosis inhibitor ZVAD (39), whereas UV-induced pan-nuclear γH2AX was not, although ZVAD did suppress apoptotic detachment (15). Thus, pan-nuclear H2AX might occur earlier on the apoptotic pathway after UV irradiation than after TRAIL activation. JNK-mediated phosphorylation of H2AX was essential for caspase-activated DNase (CAD)-mediated nucleosomal DNA fragmentation during apoptosis (19), which suggests that UV-induced pan-nuclear γH2AX may be essential for early steps before CAD-mediated nucleosomal DNA fragmentation. High levels of pan-nuclear γH2AX could correspond to a genome-wide modification in chromatin conformation, increasing the accessibility of nucleosomal DNA to the CAD endonuclease (19) and H2AX kinases.

Although ATR is the main kinase activated in response to replication stress after UV irradiation (6), we found that ATM, rather than ATR, mediated the UV-induced pan-nuclear γH2AX and apoptosis during S phase. ATR may not, therefore, generate high levels γH2AX during UV-induced replication stress. Inhibition of ATR by caffeine (32), however, increased both the UV-induced pan-nuclear γH2AX (Fig. 2*A* and Fig. S3) and apoptosis during S phase (Fig. 4*C* and Fig. S4), especially in Pol η-deficient cells (Fig. 2*C*). Instead, ATR's role might be to mediate a UV-induced survival pathway in which γH2AX plays a minimal role; inhibition of ATR would then divert cells to an ATM- and JNK-dependent apoptotic pathway associated with high levels of γH2AX. Previous studies have shown that inhibition of the ATR–Chk1 pathway by caffeine promoted apoptosis after UV (32) and increased cell death in the S phase (36), especially in Pol η-deficient cells (40). We, therefore, propose that three pathways might compete for cell fate after UV irradiation during S phase: a Pol η-dependent translesional synthesis pathway, an ATR-dependent survival pathway that becomes more important in the absence of Pol η, and an ATM/JNK-dependent apoptotic pathway that involves high levels of pan-nuclear γH2AX. The requirement of XPA and XPC for high levels of γH2AX and fork breakage could imply that there is conflict between excision repair and DNA replication that is potentially lethal in S phase.

This study highlights the complexity of the UV-induced γH2AX response and calls into question the widely accepted correspondence between γH2AX and DSBs (13–16). We have shown that UV-induced DSBs, measured by colocalization of large γH2AX and 53BP1 foci, represented less than one-half the total number of γH2AX foci that were detected. The formation of γH2AX foci after treatment with DNA-damaging agents could not, therefore, be used as a direct measure of DSBs without independent corroborating evidence.

Materials and Methods

Cell Culture. A series of normal and repair- or replication-deficient human fibroblast cell lines, transformed with either SV40 or hTERT, were used (Table S1). SV40-transformed cells were used to investigate apoptosis, because, unlike hTERT-transformed cells, high levels of p53 cause cells to detach from the growth surface after UV irradiation, allowing quantification of S phase apoptosis (41, 42).

Immunohistochemistry and FACS Analysis of γH2Ax and 53BP1. Detection of γH2Ax and 53BP1 by IF and FACS analysis was carried out as described previously (15, 20, 35); full details are provided in *SI Materials and Methods*. The antibodies used were mouse monoclonal γH2AX (Ser-139), 1:1,000 (Upstate Biotechnology); rabbit polyclonal γH2Ax (Ser-139), 1:1,000 (Novus Biologicals); rabbit polyclonal 53BP1, 1:300 (Cell signaling, #4937), anti-phospho-Chk2 (Thr68; #2661; Cell Signaling); and anti-PCNA (FL-261; #2661; Santa Cruz), 1:200. For double staining, antibodies to γH2AX and 52BP1 were applied together on cells fixed with 4% paraformaldehyde or 100% methanol.

Apoptosis. Apoptosis was measured by growing cells to 75% confluence, irradiating them with 20 J/m^2, and incubating them for 20 h in medium supplemented with ZVAD (1–100 μM), JNK inhibitor SP600125 (100 μM), or ATM inhibitor KU55933 (50 μM). Between 3 and 12 different experiments were conducted for each cell line and treatment. For each experiment, controls and treated cells were run in parallel. The percentage of apoptotic cells released from the substrate was calculated as the number of detached cells divided by the total number of attached plus detached cells (15, 35) (Fig. S4). ZVAD, KU55933, and SP600125 are cytotoxic, and we observed a small increase in detached cells in the presence rather than the absence of these compounds in nonirradiated cells. To compensate for this nonspecific toxicity in UV-irradiated cells, we normalized the percentage of detached cells by subtracting the percentage of nonirradiated detached cells from the percentage of UV-irradiated detached cells.

Statistics. Data were compared using ANOVA (single factor) and one-tailed *t* tests (two-sample assuming unequal variances) with a hypothesized mean difference of 0 and $\alpha = 5\%$.

ACKNOWLEDGMENTS. We thank the University of California San Francisco Helen Diller Family Comprehensive Cancer Center cell analysis core facility, Steven I. Reed and Boris Bastian's laboratory for technical assistance, Louise Lutze-Man, Mike Fried, and Donna Albertson for proof reading, and Gerard Evan and Allan Balmain for suggestions. We are also grateful to the Xeroderma Pigmentosum Society and the Luke O'Brien Foundation for their continued support and encouragement for the University of California San Francisco research program. This research was funded by the National Institute of Neurological Disorders and Stroke Grant R01NS052781 from the National Institutes of Health (to J.E.C.), National Institute of Arthritis and Musculoskeletal and Skin Grant P01AR050440 from the National Institutes of Health, and the Cancer Center Support Grant P30 CA82103.

1. Bartkova J, et al. (2006) Oncogene-induced senescence is part of the tumorigenesis barrier imposed by DNA damage checkpoints. *Nature* 444:633–637.
2. Sancar A, Lindsey-Boltz LA, Unsal-Kaçmaz K, Linn S (2004) Molecular mechanisms of mammalian DNA repair and the DNA damage checkpoints. *Annu Rev Biochem* 73: 39–85.
3. Lee J-H, Paull TT (2005) ATM activation by DNA double-strand breaks through the Mre11-Rad50-Nbs1 complex. *Science* 308:551–554.
4. Shiloh Y (2003) ATM and related protein kinases: Safeguarding genome integrity. *Nat Rev Cancer* 3:155–168.
5. Cortez D, Guntuku S, Qin J, Elledge SJ (2001) ATR and ATRIP: Partners in checkpoint signaling. *Science* 294:1713–1716.
6. Zou L, Elledge SJ (2003) Sensing DNA damage through ATRIP recognition of RPA-ssDNA complexes. *Science* 300:1542–1548.
7. Shechter D, Costanzo V, Gautier J (2004) Regulation of DNA replication by ATR: Signaling in response to DNA intermediates. *DNA Repair (Amst)* 3:901–908.
8. Ward IM, Chen J (2001) Histone H2AX is phosphorylated in an ATR-dependent manner in response to replicational stress. *J Biol Chem* 276:47759–47762.
9. Burma S, Chen BP, Murphy M, Kurimasa A, Chen DJ (2001) ATM phosphorylates histone H2AX in response to DNA double-strand breaks. *J Biol Chem* 276: 42462–42467.
10. Falck J, Coates J, Jackson SP (2005) Conserved modes of recruitment of ATM, ATR and DNA-PKcs to sites of DNA damage. *Nature* 434:605–611.
11. Hurley PJ, Bunz F (2007) ATM and ATR: Components of an integrated circuit. *Cell Cycle* 6:414–417.
12. Abraham RT (2001) Cell cycle checkpoint signaling through the ATM and ATR kinases. *Genes Dev* 15:2177–2196.
13. Xie A, et al. (2007) Distinct roles of chromatin-associated proteins MDC1 and 53BP1 in mammalian double-strand break repair. *Mol Cell* 28:1045–1057.
14. Stewart GS, Wang B, Bignell CR, Taylor AM, Elledge SJ (2003) MDC1 is a mediator of the mammalian DNA damage checkpoint. *Nature* 421:961–966.
15. Limoli CL, Giedzinski E, Morgan WF, Cleaver JE (2000) Inaugural article: Polymerase eta deficiency in the xeroderma pigmentosum variant uncovers an overlap between the S phase checkpoint and double-strand break repair. *Proc Natl Acad Sci USA* 97: 7939–7946.
16. Fernandez-Capetillo O, et al. (2002) DNA damage-induced G2-M checkpoint activation by histone H2AX and 53BP1. *Nat Cell Biol* 4:993–997.
17. Fernandez-Capetillo O, et al. (2003) H2AX is required for chromatin remodeling and inactivation of sex chromosomes in male mouse meiosis. *Dev Cell* 4:497–508.
18. Fernandez-Capetillo O, Lee A, Nussenzweig M, Nussenzweig A (2004) H2AX: The histone guardian of the genome. *DNA Repair (Amst)* 3:959–967.
19. Lu C, et al. (2006) Cell apoptosis: Requirement of H2AX in DNA ladder formation, but not for the activation of caspase-3. *Mol Cell* 23:121–132.
20. Marti TM, Hefner E, Feeney L, Natale V, Cleaver JE (2006) H2AX phosphorylation within the G1 phase after UV irradiation depends on nucleotide excision repair and not DNA double-strand breaks. *Proc Natl Acad Sci USA* 103:9891–9896.
21. Squires S, et al. (2004) p53 prevents the accumulation of double-strand DNA breaks at stalled-replication forks induced by UV in human cells. *Cell Cycle* 3:1543–1557.
22. Limoli CL, Giedzinski E, Bonner WM, Cleaver JE (2002) UV-induced replication arrest in the xeroderma pigmentosum variant leads to DNA double-strand breaks, gamma -H2AX formation, and Mre11 relocalization. *Proc Natl Acad Sci USA* 99:233–238.
23. Limoli CL, Giedzinski E, Cleaver JE (2005) Alternative recombination pathways in UV-irradiated XP variant cells. *Oncogene* 24:3708–3714.
24. Masutani C, et al. (1999) The XPV (xeroderma pigmentosum variant) gene encodes human DNA polymerase eta. *Nature* 399:700–704.
25. Johnson RE, Kondratick CM, Prakash S, Prakash L (1999) hRAD30 mutations in the variant form of xeroderma pigmentosum. *Science* 285:263–265.
26. Ward IM, Minn K, Jordan KG, Chen J (2003) Accumulation of checkpoint protein 53BP1 at DNA breaks involves its binding to phosphorylated histone H2AX. *J Biol Chem* 278:19579–19582.
27. Schultz LB, Chehab NH, Malikzay A, Halazonetis TD (2000) p53 binding protein 1 (53BP1) is an early participant in the cellular response to DNA double-strand breaks. *J Cell Biol* 151:1381–1390.
28. Muslimović A, Nyström S, Gao Y, Hammarsten O (2009) Numerical analysis of etoposide induced DNA breaks. *PLoS One* 4:e5859.
29. Donà F, et al. (2008) Loss of histone H2AX increases sensitivity of immortalized mouse fibroblasts to the topoisomerase II inhibitor etoposide. *Int J Oncol* 33:613–621.
30. Smart DJ, et al. (2008) Assessment of DNA double-strand breaks and gammaH2AX induced by the topoisomerase II poisons etoposide and mitoxantrone. *Mutat Res* 641: 43–47.
31. Sarkaria JN, et al. (1999) Inhibition of ATM and ATR kinase activities by the radiosensitizing agent, caffeine. *Cancer Res* 59:4375–4382.
32. Heffernan TP, et al. (2009) ATR-Chk1 pathway inhibition promotes apoptosis after UV treatment in primary human keratinocytes: Potential basis for the UV protective effects of caffeine. *J Invest Dermatol* 129:1805–1815.
33. Limoli CL, Laposa R, Cleaver JE (2002) DNA replication arrest in XP variant cells after UV exposure is diverted into an Mre11-dependent recombination pathway by the kinase inhibitor wortmannin. *Mutat Res* 510:121–129.
34. Maillard O, Solyom S, Naegeli H (2007) An aromatic sensor with aversion to damaged strands confers versatility to DNA repair. *PLoS Biol* 5:e79.
35. Cleaver JE, et al. (2002) Polymerase eta and p53 jointly regulate cell survival, apoptosis and Mre11 recombination during S phase checkpoint arrest after UV irradiation. *DNA Repair (Amst)* 1:41–57.
36. Domon M, Rauth AM (1969) Effects of caffeine on ultraviolet-irradiated mouse L cells. *Radiat Res* 39:207–221.
37. Rothkamm K, Löbrich M (2003) Evidence for a lack of DNA double-strand break repair in human cells exposed to very low X-ray doses. *Proc Natl Acad Sci USA* 100: 5057–5062.
38. Painter RB, Jermany DA, Rasmussen RE (1966) A method to determine the number of DNA replicating units in cultured mammalian cells. *J Mol Biol* 17:47–56.
39. Solier S, Sordet O, Kohn KW, Pommier Y (2009) Death receptor-induced activation of the Chk2- and histone H2AX-associated DNA damage response pathways. *Mol Cell Biol* 29:68–82.
40. Arlett CF, Harcourt SA, Broughton BC (1975) The influence of caffeine on cell survival in excision-proficient and excision-deficient xeroderma pigmentosum and normal cell strains following ultraviolet-light irradiation. *Mutat Res* 33:341–346.
41. Cleaver JE, et al. (1999) Increased ultraviolet sensitivity and chromosomal instability related to P53 function in the xeroderma pigmentosum variant. *Cancer Res* 59: 1102–1108.
42. Laposa RR, Feeney L, Crowley E, de Feraudy S, Cleaver JE (2007) p53 suppression overwhelms DNA polymerase eta deficiency in determining the cellular UV DNA damage response. *DNA Repair (Amst)* 6:1794–1804.